

High CO₂/N₂/O₂/CO Separation in a Chemically Robust Porous Coordination Polymer with Low Binding Energy

Jingui Duan,^a Masakazu Higuchi,^a Rajamani Krishna,^b Tomokazu Kiyonaga,^a Yosuke Tsutsumi,^c Yohei Sato,^d Yoshiki Kubota,^{d,e} Masaki Takata,^e and Susumu Kitagawa^{*a,c}

^a Institute for Integrated Cell-Material Sciences (WPI-iCeMS) , Kyoto University, Yoshida, Sakyo-ku, Kyoto 606-8501, Japan. Email: kitagawa@icems.kyoto-u.ac.jp.

^b Van 't Hoff Institute for Molecular Sciences, University of Amsterdam, Science Park 904, 1098 XH Amsterdam, The Netherlands.

^c Department of Synthetic Chemistry and Biological Chemistry, Graduate School of Engineering, Kyoto University, Katsura, Nishikyo-ku, Kyoto 615-8510, Japan.

^d Department of Physical Science, Graduate School of Science, Osaka Prefecture University, Sakai, Osaka 599-8531, Japan.

^e Spring-8 Center, RIKEN 1-1-1, Kouto, Sayo-cho, Sayo-gun, Hyogo 679-5148, Japan.

Reagents and general methods

All the reagents and solvents were commercially available and used as received. The FTIR spectra were recorded in the range of 4000-400 cm^{-1} on a Nicolet ID5 ATR spectrometer. Thermal analyses were performed on a Rigaku TG8120 instruments from room temperature to 600 °C at a heating rate of 5 °C/min under flowing nitrogen. The dynamic cycling behaviours of temperature-dependent gravimetric adsorption studies were also used the same TG machine. The attached gas was changed to CO_2 from N_2 . Powder X-ray diffraction (PXRD) patterns were collected using a Bruker AXS D8 Discover powder diffractometer equipped with a Cu K α X-ray source at 40 kV, 40 mA. Simulated powder patterns from single-crystal X-ray diffraction data were generated using Mercury 1.4.2 software.

Single crystal X-ray study

All measurements were made on a Rigaku Saturn 724+ diffractometer using graphite monochromated Mo-K α radiation. The data were collected at a temperature of 173K to a maximum 2θ value of 50.2°. A total of 720 oscillation images were collected. A sweep of data was done using ω scans from -110.0 to 70.0° in 0.50° step, at $\chi = 45.0^\circ$ and $\phi = 0.0^\circ$. The exposure rate was 128.0 [sec./°]. The detector swing angle was -20.15°. A second sweep was performed using ω scans from -110.0 to 70.0° in 0.50° step, at $\chi=45.0^\circ$ and $\phi = 90.0^\circ$. The exposure rate was 128.0 [sec./°]. The detector swing angle was -20.15°. The crystal-to-detector distance was 44.95 mm. Readout was performed in the 0.141 mm pixel mode. Data were collected and processed using CrystalClear¹. The linear absorption coefficient, μ , for Mo-K α radiation is 8.987 cm^{-1} . An empirical absorption correction was applied which resulted in transmission factors ranging from 0.461 to 0.835. The data were corrected for Lorentz and polarization effects. The structure was solved by direct methods² and expanded using Fourier techniques. Some non-hydrogen atoms were refined anisotropically, while the rest were refined isotropically. Hydrogen atoms were refined using the riding model. Neutral atom scattering factors were taken from Cromer and Waber³. Anomalous dispersion effects were included in Fcalc⁴; the values for $\Delta f'$ and $\Delta f''$ were those of Creagh and McAuley⁵. The values for the mass attenuation coefficients are those of Creagh and Hubbell⁶. All calculations were performed using the CrystalStructure¹ crystallographic software package except for refinement, which was performed using SHELXL-97⁷.

Adsorption Experiments

Before the measurement, the solvent-exchanged sample (about 100 mg) was prepared by immersing the as-synthesized samples in methanol for three days to remove the nonvolatile solvents, and the extract was decanted every 8 h and fresh methanol was replaced. The completely activated sample was obtained by heating the solvent-exchanged sample at 120 °C under a dynamic high vacuum for 20 h. In the gas adsorption measurement, ultra-high-purity grade were used throughout the adsorption experiments. Gas adsorption isotherms were obtained using a Belsorp-mini volumetric adsorption instrument from BEL Japan Inc. using the volumetric technique. To provide high accuracy and precision in determining P/P_0 , the saturation pressure P_0 was measured throughout the N_2 analyses by means of a dedicated saturation pressure transducer, which allowed us to monitor the vapor pressure for each data point.

Moisture and chemical stability experiments

About moisture experiment, approximately 50 mg of degassed PCP-1 samples were treated in the oven with different conditions (25°C, 80%RH, 50°C, 80%RH and 100°C, 80%RH,) for 24h, respectively. After the temperature cool down, partial samples were used for PXRD patterns collections and partial samples were used for gas sorption works (degassed at 120°C for 24h). For chemical treatment, fresh PCP-1 was soaked (around 50-60 mg for each) into three bottles (4 ml). HCl and NaOH were used to turn the pH of the solution to 2, 7 and 12. The bottles were heated to 100°C for 24h. After the temperature cool down, partial samples were used for PXRD patterns collections and partial samples were used for gas sorption works (washed by methanol three times and degassed at 120°C for 24h).

Fitting of pure component isotherms

The experimentally measured excess loadings of CO_2 , CO , O_2 , and N_2 obtained at temperatures at 195 K and 273 K were first converted to absolute loadings before data fitting. For this purpose the pore volume used is 0.1218 cm³/g. It generated from the N_2 adsorption experiment. The procedure for converting excess loadings to absolute loadings is described in detail in the Supporting Information accompanying Wu et al.⁸

The isotherm data at both temperatures were fitted with the Langmuir-Freundlich model

$$q = q_{sat} \frac{bp^v}{1 + bp^v} \quad (1)$$

with T -dependent parameter b

$$b_A = b_0 \exp\left(\frac{E}{RT}\right) \quad (2)$$

The Langmuir-Freundlich parameters for adsorption of CO₂, CO, O₂, and N₂ in PCP-1 are provided in Table 1.

Isosteric heat of adsorption

For use of PCP-1 in a pressure swing adsorption device, the isosteric heat of adsorption of CO₂ is important, because it largely dictates the energy required in the regeneration cycle. The isosteric heat, Q_{st} , defined as

$$Q_{st} = RT^2 \left(\frac{\partial \ln p}{\partial T} \right)_q \quad (3)$$

were determined using the pure component isotherm fits. The calculations of, Q_{st} , are based on the use of the Clausius-Clapeyron equation. The data for other materials have been collected from a variety of sources.⁸⁻¹¹

In order to get the precise information of the isosteric heat of CO₂ in PCP-1, a virial-type¹² expression comprising the temperature-independent parameters a_i and b_i was employed to calculate the enthalpies of adsorption for CO₂ (at 263, 273 and 283K) on PCP-1. In each case, the data were fitted using the equation:

$$\ln P = \ln N + 1/T \sum_{i=0}^m a_i N^i + \sum_{i=0}^n b_i N^i \quad (4)$$

Here, P is the pressure expressed in Torr, N is the amount adsorbed in mmol/g, T is the temperature in K, a_i and b_i are virial coefficients, and m , n represent the number of coefficients required to adequately describe the isotherms (m and n were gradually increased until the contribution of extra added a and b coefficients was deemed to be statistically insignificant towards the overall fit, and the average value of the squared deviations from the experimental values was minimized).

$$Q_{st} = -R \sum_{i=0}^m a_i N^i \quad (5)$$

Here, Q_{st} is the coverage-dependent isosteric heat of adsorption and R is the universal gas constant.

Calculations of adsorption selectivity

The selectivity of preferential adsorption of component 1 over component 2 in a mixture containing 1 and 2, perhaps in the presence of other components too, can be formally defined as

$$S_{ads} = \frac{q_1/q_2}{p_1/p_2} \quad (6)$$

In equation (6), q_1 and q_2 are the *absolute* component loadings of the adsorbed phase in the mixture. In all the calculations to be presented below, the calculations of S_{ads} are based on the use of the Ideal Adsorbed Solution Theory¹³ of Myers and Prausnitz.¹⁴

Temperature-programmed desorption (TPD) of NH₃

Evacuated PCP-1 (30mg) was loaded in the center of the U-type cell. The system was then degassed at 100°C for 5h. After the temperature cool down, NH₃ gas (26 ml/min) was introduced to pass through the cell for 30mins. In order to wash the free NH₃, the He gas (30 ml/min) was used to blow the cell for another 60mins. The TPD data were collected using a heating rate of 5 K/min under He (30 mL/min) with Q-mass ($m/z = 16$) as a detector.

Packed bed absorber breakthrough simulations

The separation of CO₂/CO/O₂/N₂ gas mixtures is carried out in fixed bed adsorption units. In order to demonstrate the separation potential of PCP-1, we performed breakthrough simulations using the methodology described in earlier works.^{8-11, 15-17} Experimental validation of the breakthrough simulation methodology is available in the published literature.^{8, 10, 18, 19} Fig. S15 shows a schematic of a packed bed adsorber packed with PCP-1. The following parameter values were used: length of packed bed, $L = 0.1$ m; fractional voidage of packed bed, $e = 0.4$; superficial gas velocity at inlet of adsorber, $u = 0.04$ m/s, framework density of PCP-1, $r = 974$ kg/m³. The inlet gas is a quaternary mixture CO₂/CO/O₂/N₂ at 100 kPa, with partial pressures for each component of 25 kPa. The x -axis in is dimensionless time dimensionless time, t , defined by dividing the actual time, t , by the

characteristic time, $\frac{L\varepsilon}{u}$.

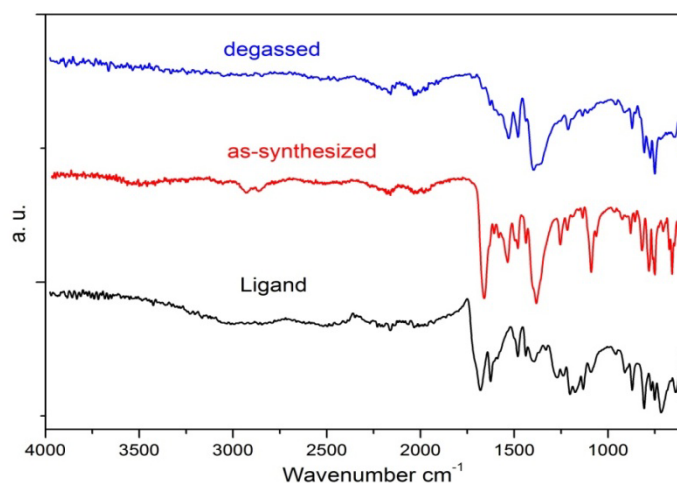


Fig. S1 Infrared spectra. (a) H₃BTN, (b) as-synthesized PCP-1, (c) activated PCP-1. Note the absence of the vibration frequencies of the solvent DMF and methanol molecules in the activated samples.

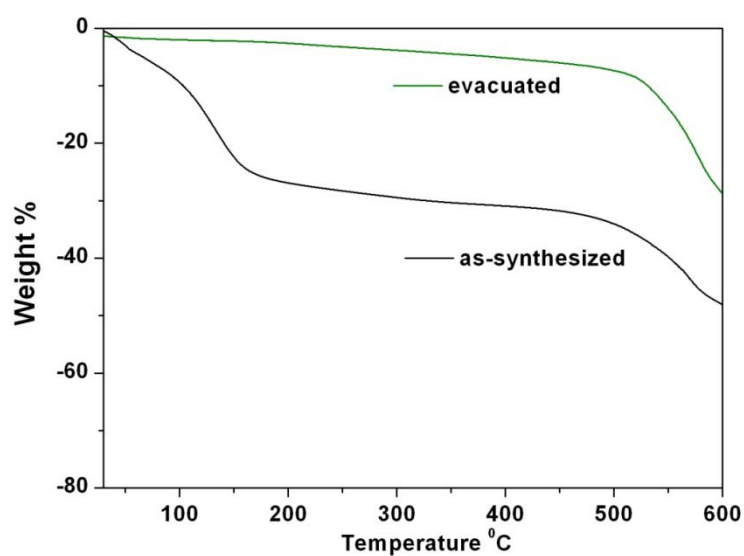


Fig. S2 TG of PCP-1: as-synthesized samples and completely activated samples (green).

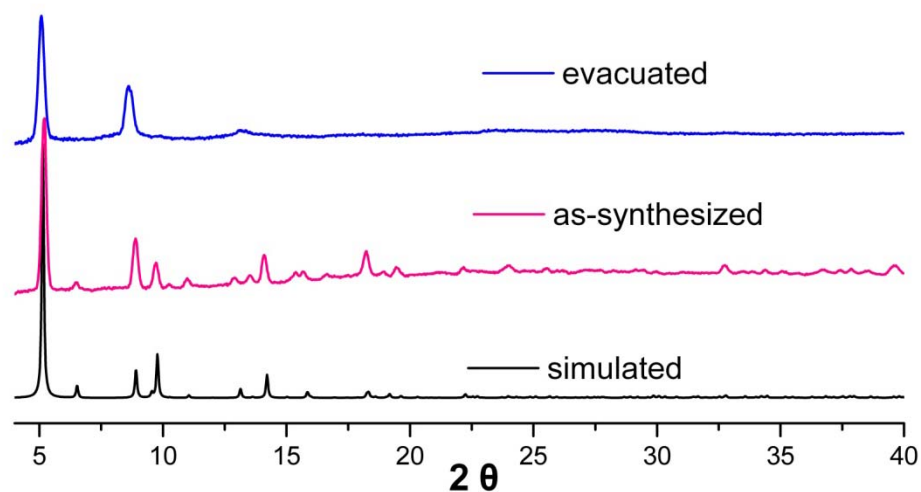


Fig. S3 The PXRD patterns of PCP-1: as-synthesized, completely activated samples and the activated samples treated at varied environment along with the simulated XRD pattern from the single crystal data.

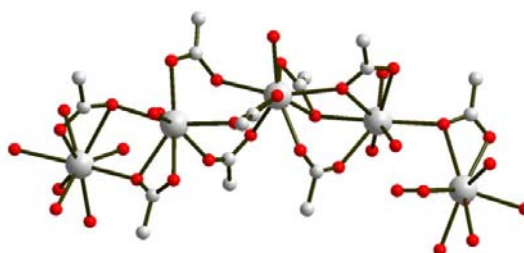


Fig. S4 The coordination connection of metal-oxygen chain in PCP-1.

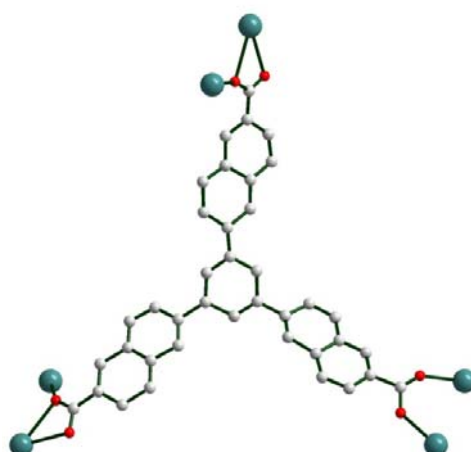


Fig. S5 Two different coordination modes ($\mu_2-\eta^1:\eta^1$, $\mu_2-\eta^2:\eta^1$) of three carboxylate groups of BTN ligand (b).

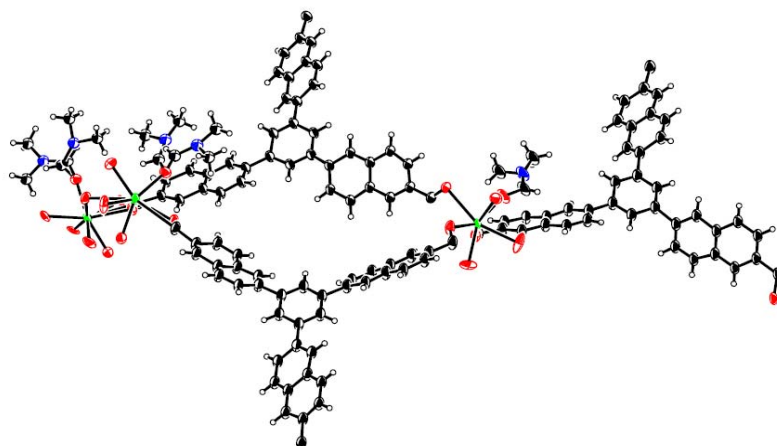


Fig. S6 Molecular structure of PCP-1. Thermal ellipsoids are drawn at 30% probability.

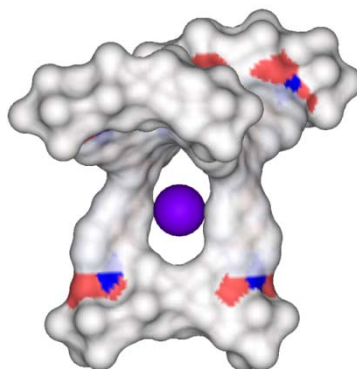


Fig. S7 The Connolly surface diagram and the purple ball display the space between two adjacent BTN ligands in PCP-1.

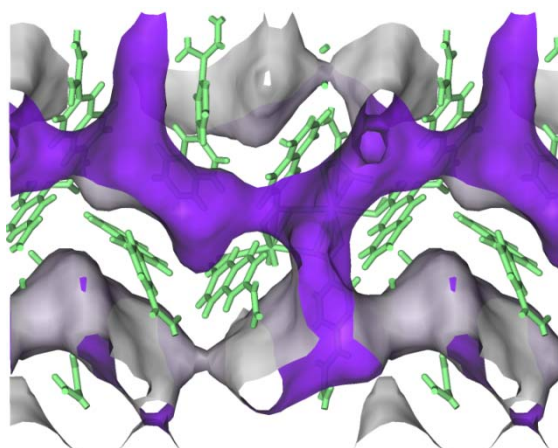


Fig. S8 The Connolly surface diagram displays the irregular channels of PCP-1 (inner surfaces: pink, outer surfaces: grey).

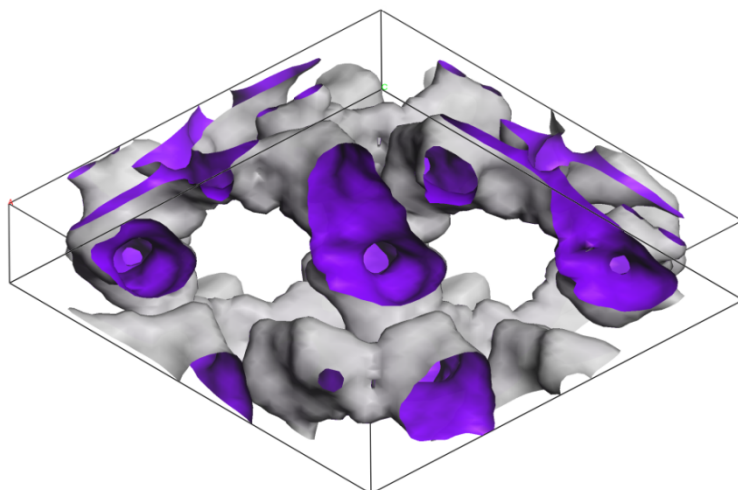


Fig. S9 The Connolly surface diagram displays the two dimensional irregular tunnels of PCP-1 (inner surfaces: pink, outer surfaces: grey).

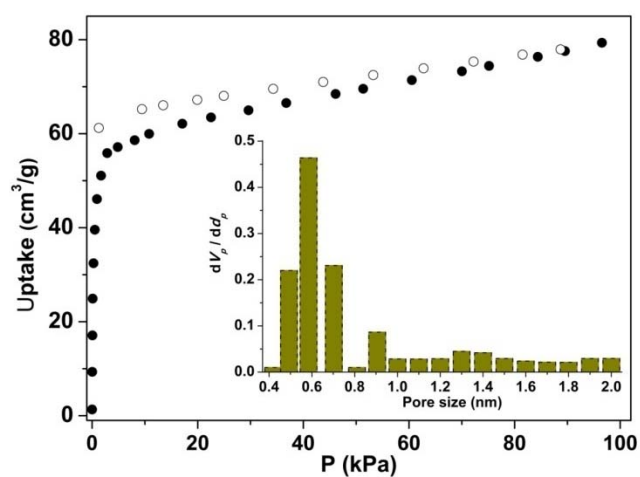


Fig. S10 N_2 adsorption isotherm and pore size distributions of PCP-1 at 77 K.

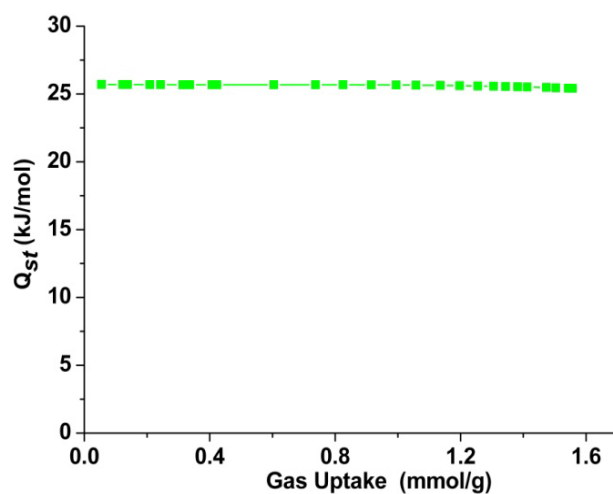


Fig. S11 Isosteric heat of CO_2 adsorption for PCP-1 at low surface coverage.

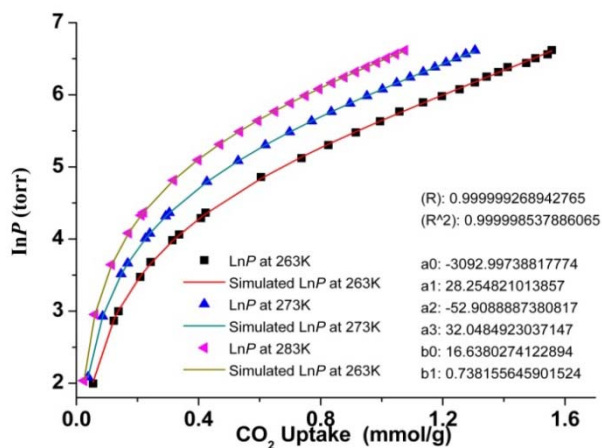


Fig. S12 The calculated virial equation isotherms parameters fit to the experimental CO₂ data of PCP-1.

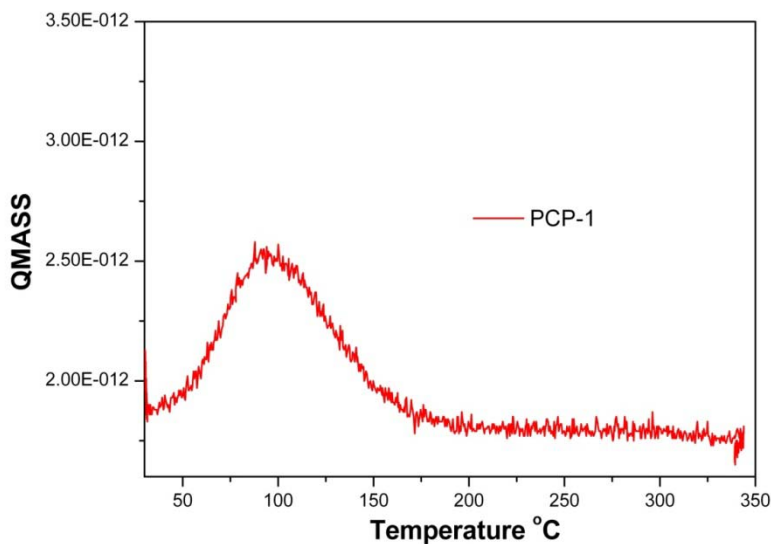


Fig. S13 NH₃-TPD result of PCP-1.

Table S1 Comparison of NH₃-TPD results of PCP-1 and other PCPs.

PCP	T _{des} (°C)	D (mmol/g)	obsd / calcd
MIL-101(Cr) ²⁰	260	2.91 / 2.94	
La-BTTc ²¹	430	1.39 / 1.69	
PCP-1	95	0.52 / 1.25	

Table S2 List of physical and electronic parameters for the adsorbate molecules





	CO ₂	O ₂	N ₂	CO
				
Kinetic diameter (Å)	3.3	3.46	3.64	3.76
Dipole moment (D)	0	0	0	0.117
Quadruple moment 10 ⁴⁰ θ (cm ²)	13.4	1.3	4.7	8.3
Polarizability (Å ³)	2.65	1.60	1.76	1.95

Table S3 Langmuir-Freundlich parameters for adsorption of CO₂, CO, O₂, and N₂ in PCP-1. The isotherm fits are based on data obtained at 195 K and 273 K. The experimentally measured excess loadings were first converted to absolute loadings before data fitting.

	q_{sat} mol kg ⁻¹	b_0 Pa ^{-ν}	E kJ mol ⁻¹	ν dimensionless
CO ₂	3.9	7.26×10 ⁻⁹	21.4	0.75
CO	1.7	4.18×10 ⁻¹⁰	17.7	1
O ₂	1.8	1.15×10 ⁻⁹	15	1
N ₂	1.6	6.94×10 ⁻¹⁰	16	1

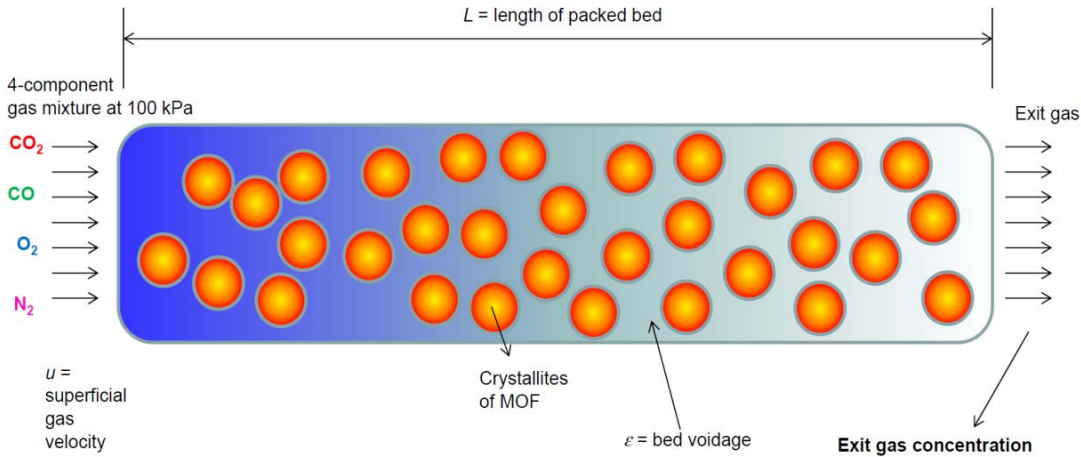


Fig. S14 Schematic of a packed bed adsorber.

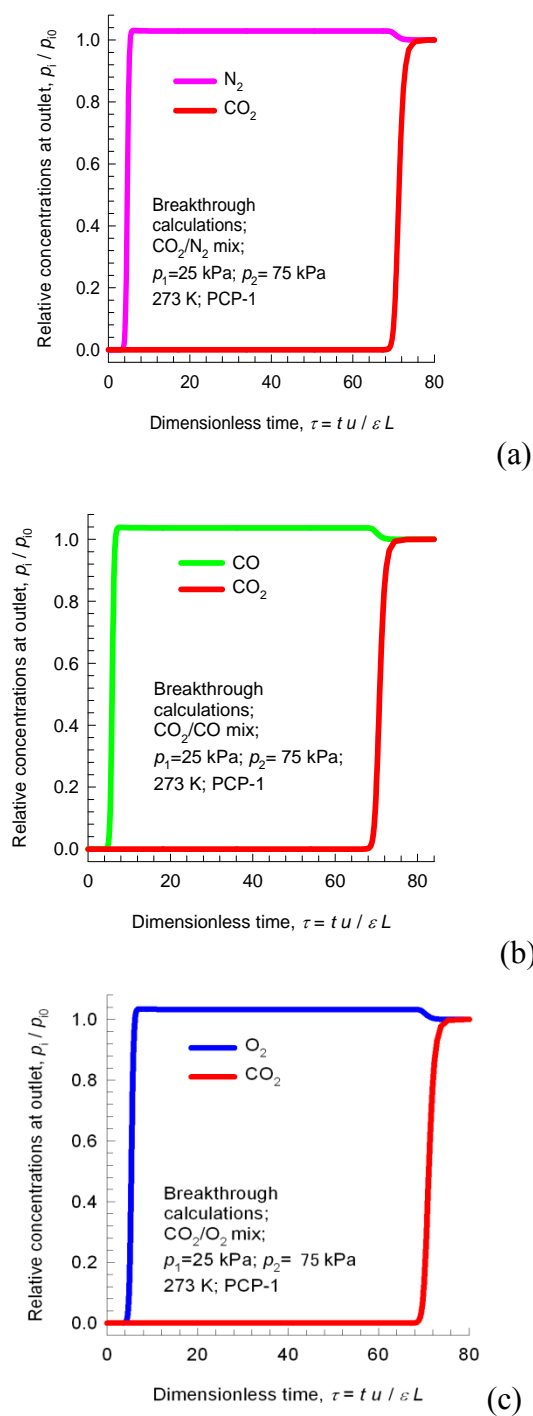


Fig. S15 Breakthrough characteristics of adsorber packed with PCP-1 and maintained at isothermal conditions at 273 K. The inlet gas is a binary mixture (a) CO₂/CO, (b) CO₂/O₂, and (c) CO₂/N₂ at 100 kPa. The partial pressure of CO₂ in all three cases is maintained at 25 kPa.

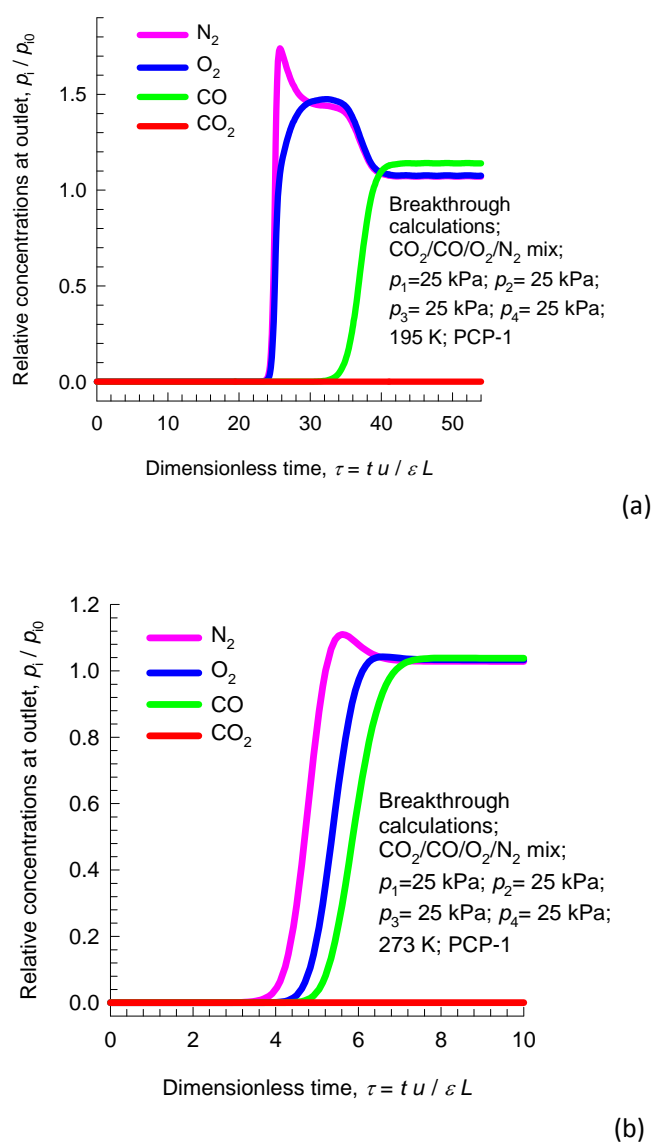


Fig. S16 Breakthrough characteristics of an adsorber packed with PCP-1 and maintained at isothermal conditions at 195 K and 273K, respectively. The inlet gas is a quaternary mixture $CO_2/CO/O_2/N_2$ at 100 kPa, with partial pressures for each component of 25 kPa. The data shown in (a: 195K and b: 273K) are for the shorter times in order to highlight the breakthrough of the more poorly adsorbed components.

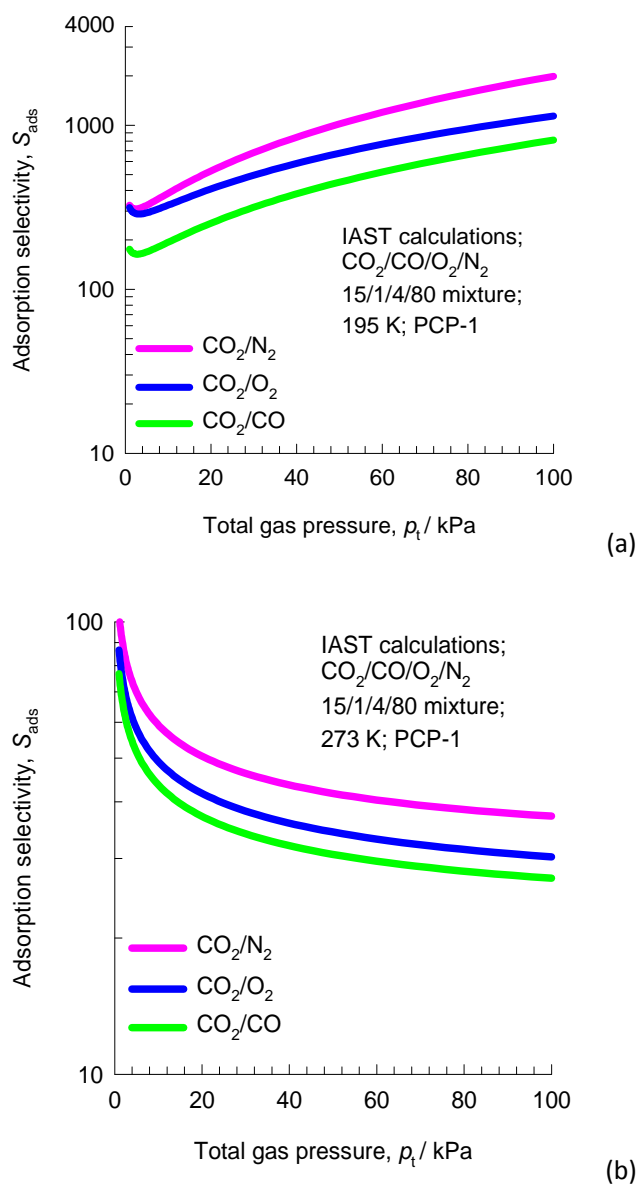
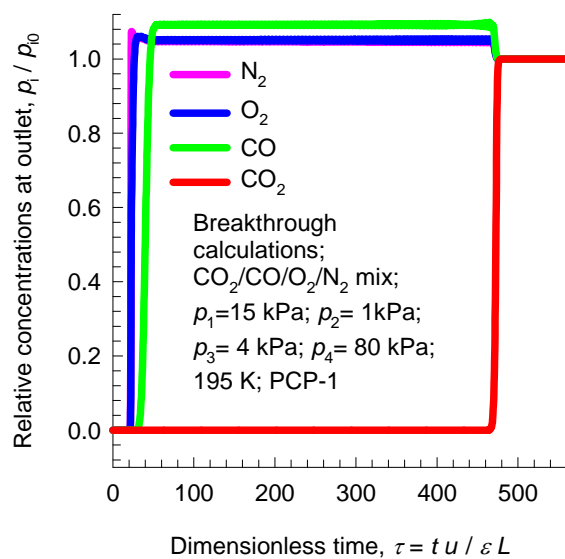
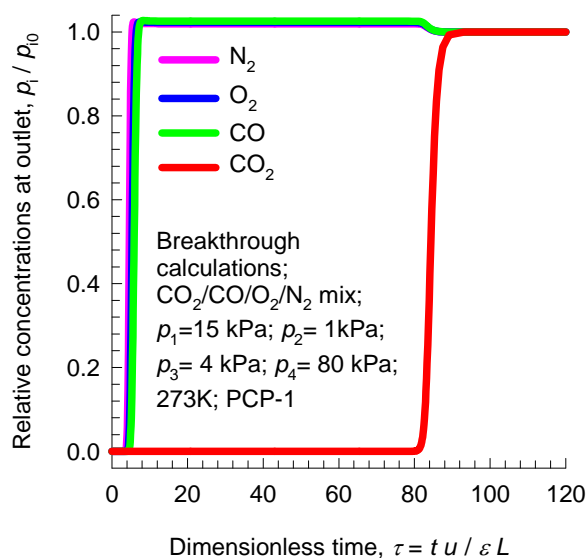


Fig. S17 Calculations using Ideal Adsorbed Solution Theory (IAST) of Myers and Prausnitz for CO_2/CO , CO_2/O_2 , and CO_2/N_2 selectivities for 15/1/4/80 $\text{CO}_2/\text{CO}/\text{O}_2/\text{N}_2$ gas mixtures maintained at isothermal conditions at (a) 195 K, and (b) 273 K.



(a)



(b)

Fig. S18 Breakthrough characteristics of an adsorber packed with PCP-1 and maintained at isothermal conditions at 195 K (a) and 273 K (b). The inlet gas is a 15/1/4/80 CO₂/CO/O₂/N₂ quaternary mixture at 100 kPa.

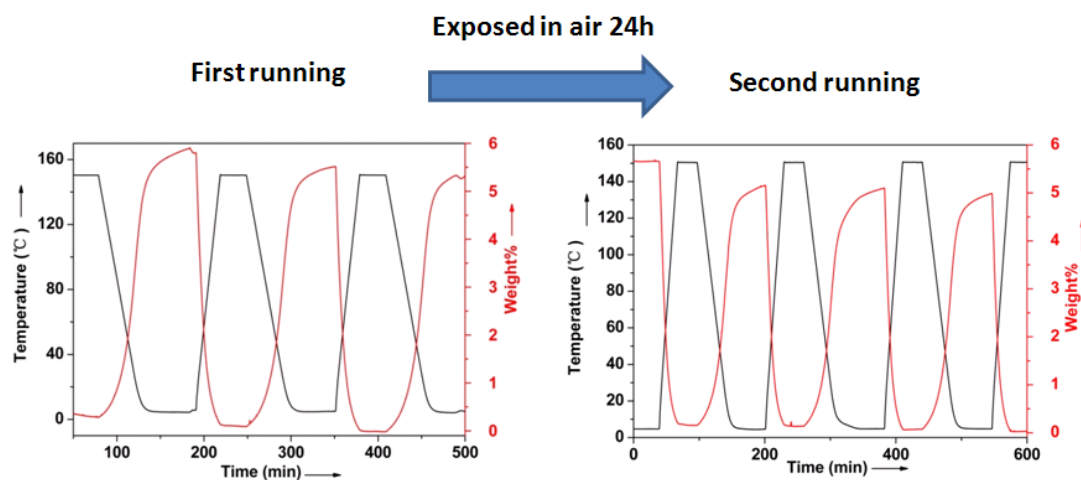


Fig. S19 Dynamic adsorption studies of PCP-1 using TGA. Experimental mass changes are shown in pure CO₂ (red circles).

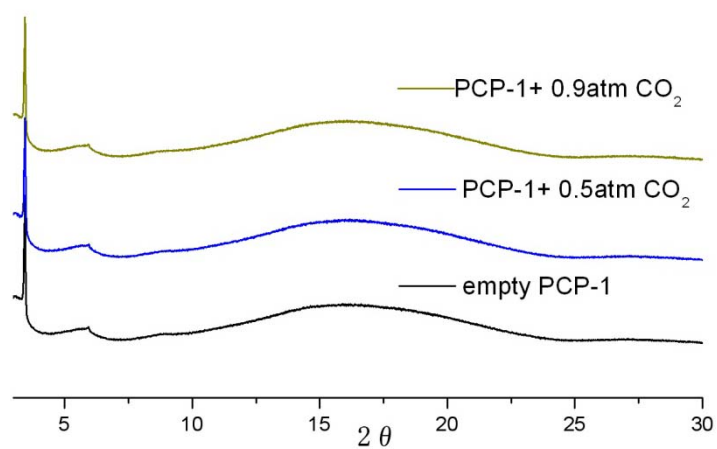


Fig. S20 The powder synchrotron X-ray diffraction pattern of PCP-1 with CO₂ at different pressure.

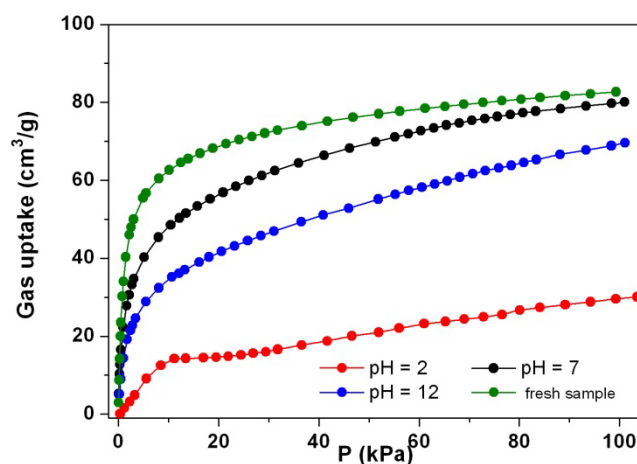


Fig. S21 CO₂ adsorption profiles of PCP-1 before and after chemical treatment. (Desorption were omitted for clearly, as all of them show complete desorption.)

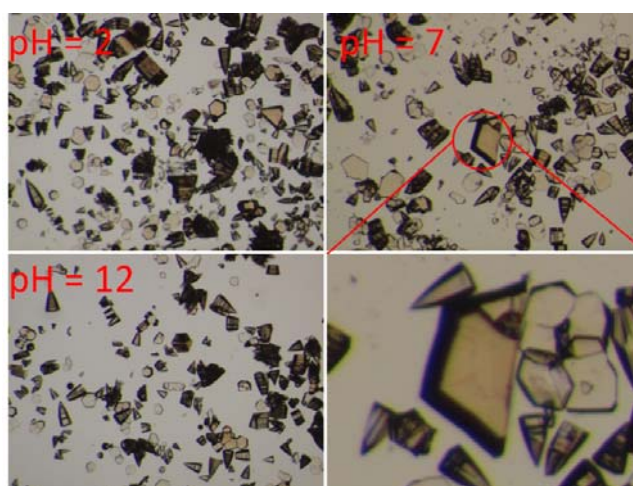


Fig. S22 Photos of PCP-1 indicate the crystalline after water treatment at different pH and 100 °C for 24h.

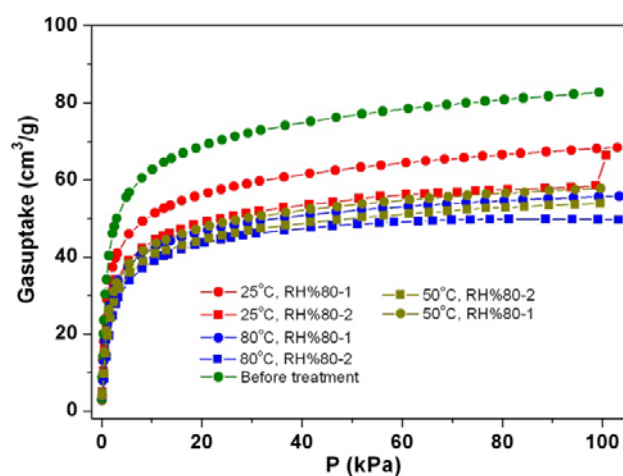


Fig. S23 CO₂ adsorption of PCP-1 before and after moisture treatment (Desorption were omitted for clearly, as all of them show complete desorption).

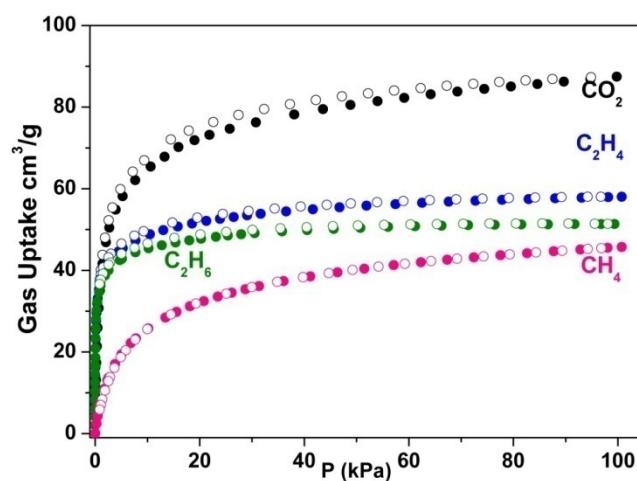


Fig. S24 Adsorption isotherms of energy gas in PCP-1 at 195 K.

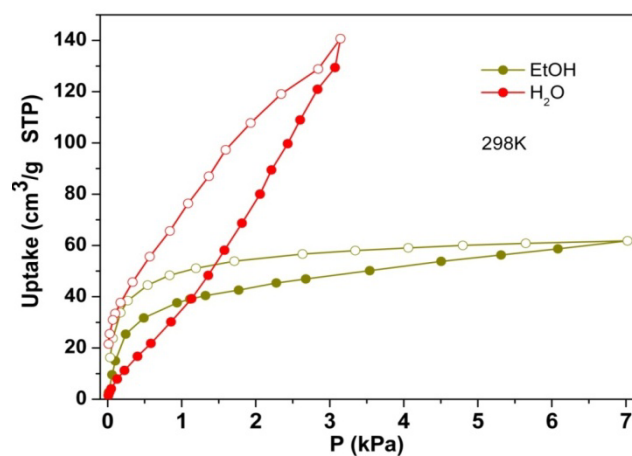


Fig. S25 Adsorption isotherms of ethanol and water in PCP-1 at 298 K.

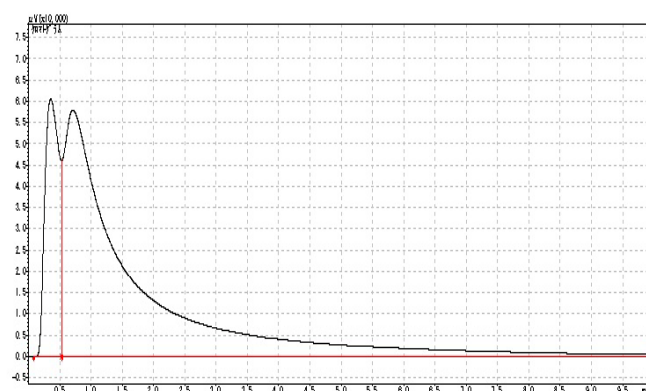


Fig. S26 This figure shows the separation of EtOH/H₂O=1:1 (1ul) at 220°C on GC. The column (radius: 2mm, length: 20cm) with degassed PCP-1 (15cm) was used (left peak is EtOH and right one is H₂O).

Notation

b	Langmuir-Freundlich constant, $\text{Pa}^{-\nu}$
L	length of packed bed adsorber, m
p_i	partial pressure of species i in mixture, Pa
p_t	total system pressure, Pa
q_i	component molar loading of species i , mol kg^{-1}
q_t	total molar loading in mixture, mol kg^{-1}
q_{sat}	saturation loading, mol kg^{-1}
Q_{st}	isosteric heat of adsorption, J mol^{-1}
R	gas constant, $8.314 \text{ J mol}^{-1} \text{ K}^{-1}$
S_{ads}	adsorption selectivity, dimensionless
t	time, s
T	absolute temperature, K
u	superficial gas velocity in packed bed, m s^{-1}
z	distance along the adsorber, m

Greek letters

ε	voidage of packed bed, dimensionless
ν	exponent in Langmuir-Freundlich isotherm, dimensionless
ρ	framework density, kg m^{-3}
τ	time, dimensionless

Reference

1. R. C.-T.-. CrystalStructure 4.1: Crystal Structure Analysis Package, Japan.
2. M. C. Burla;, R. Caliandro;, M. Camalli;, B. Carrozzini;, G. L. Cascarano;, L. D. Caro;, C. Giacovazzo, G. Polidori, D. Siliqi and R. Spagna, *SIR2008*, 2007.
3. D. T. W. Cromer, J. T.; "International Tables for X-ray Crystallography", Vol. IV, The Kynoch Press, Birmingham, England, Table 2.2 A, 1974.
4. J. A. Ibers and W. C. Hamilton, *Acta Crystallogr*, 1964, **17**, 781-&.
5. D. C. M. Creagh, W.J. .; "International Tables for Crystallography", Vol C, (A.J.C. Wilson, ed.), Kluwer Academic Publishers, Boston, Table 4.2.6.8, 1992, 219-222.
6. D. C. H. Creagh, J.H.; "International Tables for Crystallography", Vol C, (A.J.C. Wilson, ed.), Kluwer Academic Publishers, Boston, Table 4.2.4.3, pages 200-206 (1992). .
7. G. M. Sheldrick, *Acta Crystallographica Section A* 2008, **64**, 112-122.
8. H. Wu, K. Yao, Y. Zhu, B. Li, Z. Shi, R. Krishna and J. Li, *J. Phys. Chem. C*, 2012, **116**, 16609-16618.
9. S. C. Xiang, Y. He, Z. Zhang, H. Wu, W. Zhou, R. Krishna and B. Chen, *Nat. Commun.*, 2012, **3**, 954.
10. Y. He, R. Krishna and B. Chen, *Energy Environ. Sci.*, 2012, **5**, 9107-9120.
11. Y. He, S. Xiang, Z. Zhang, S. Xiong, C. Wu, W. Zhou, T. Yildirim, R. Krishna and B. Chen, *J. Mater. Chem. A*, 2013, **1**, 2543-2551.
12. J. L. C. Rowsell and O. M. Yaghi, *Journal of the American Chemical Society* 2006, **128**,

1304-1315.

13. J. H. Jang, M. Iastrebnier, G. Taborda, J. Arbelbide, F. Sackmann, G. Klein, H. Bernard, C. Jozami, K. Kim, D. Kim and C. Jung, *Haematologica-the Hematology Journal* 2010, **95**, 553-554.
14. A. L. Myers and J. M. Prausnitz, *A.I.Ch.E.J.*, 1965, **11**, 121-130.
15. R. Krishna and J. R. Long, *J. Phys. Chem. C*, 2011, **115**, 12941-12950.
16. R. Krishna and J. M. van Baten, *Sep. Purif. Technol.*, 2012, **87**, 120-126.
17. R. Krishna and R. Baur, *Sep. Purif. Technol.*, 2003, **33**, 213-254.
18. E. D. Bloch, W. L. Queen, R. Krishna, J. M. Zadrozny, C. M. Brown and J. R. Long, *Science*, 2012, **335**, 1606-1610.
19. Z. R. Herm, B. M. Wiers, J. M. Van Baten, M. R. Hudson, P. Zajdel, C. M. Brown, N. Maschiocchi, R. Krishna and J. R. Long, *Science*, 2013, **340**, 960-964.
20. Y. Y. Pan, B. Z. Yuan, Y. W. Li and D. H. He, *Chem. Commun.*, 2010, **46**, 2280-2282.
21. T. Kajiwara, M. Higuchi, A. Yuasa, H. Higashimura and S. Kitagawa, *Chem. Commun.*, 2013, DOI: 10.1039/C3CC43384F, .